

# GLOBAL HYBRID SIMULATIONS OF SOLAR WIND INTERACTION WITH MERCURY: MAGNETOSPHERIC BOUNDARIES

N. Omidi<sup>1</sup>, X. Blanco-Cano<sup>2</sup>, C.T. Russell<sup>3</sup> and H. Karimabadi<sup>1</sup>

<sup>1</sup>*University of California San Diego, MC 0407, La Jolla, CA 92093 USA*

<sup>2</sup>*Instituto de Geofisica, UNAM, Coyoacan D.F.04510 Mexico*

<sup>3</sup>*University of California Los Angeles, Box 951567, Los Angeles, CA 92093 USA*

## ABSTRACT

The Mariner 10 observations established the presence of a magnetosphere at Mercury with general characteristics similar to that of the Earth despite a much smaller size (i.e. magnetic dipole strength) and the absence of an atmosphere/ionosphere. Observationally, a mapping between the terrestrial and hermean magnetospheric regions has been made which entails increasing the size of the planet by a factor of 8. Recently, we have used the results of global hybrid (kinetic ions, fluid electrons) simulations of solar wind interaction with magnetic dipoles of varying strength to show the existence of a spectrum of magnetospheric structures whose size and level of complexity increases with the dipole moment. A physical parameter which helps characterize these magnetospheres is  $D_p$ , the distance ahead of the dipole where the magnetic field pressure balances the solar wind dynamic pressure. Expressed in units of ion skin depth, when  $D_p \sim 20$  the interaction results in the formation of an earthlike magnetosphere. Thus the magnetosphere of Mercury with  $D_p \sim 65$  should resemble that of the Earth. However, not all magnetospheric processes in  $D_p > 20$  magnetospheres are guaranteed to be alike and possess the same spatial and temporal scales. In this paper, we use the results of global hybrid simulations, corresponding to  $D_p = 64$ , to examine the nature of the boundaries and discontinuities at the hermean magnetosphere and how they compare with the corresponding regions at the Earth.

## INTRODUCTION

Observations of Mercury by the Mariner 10 spacecraft established it as a magnetized planet whose interaction with the solar wind results in an earthlike magnetosphere albeit much smaller (see e.g. Ness et al., 1975; 1976; Russell et al. 1988; Slavin, 2004). To account for the difference in the size of the terrestrial and the hermean magnetospheres, Ogilvie et al. (1977) proposed a linear scaling law where the size of the planet is increased by a factor of 8. So for example, to obtain the position of the nose magnetopause at Mercury, normalized to its radius, one divides the corresponding value at Earth by 8. This scaling produces good correspondence between the positions of magnetospheric boundaries at the two planets. Recently, Omidi et al. (2004a) used global hybrid (kinetic ions, fluid electrons) simulations of the solar wind interaction with magnetic dipoles of varying strength to demonstrate the presence of a spectrum of magnetospheric structures. By virtue of resolving ion temporal and spatial scales, global hybrid simulations enable study of magnetospheric solutions consisting of a single whistler wake spanning just a few thousand km (tens of ion skin depth in the solar wind) to much larger and more complex earthlike structures. It was found that the parameter  $D_p$ , which corresponds to the nose position of the magnetopause normalized to ion skin depth in the solar wind, is a good indicator of the type of magnetospheric structure one obtains and that for  $D_p \sim 20$  an earthlike magnetosphere emerges. In the case of Mercury,  $D_p \sim 65-75$  and an earthlike magnetosphere is expected. We note that the  $D_p$  values at Earth and Mercury differ by a factor of  $\sim 8-10$ .

Despite similarities in structure, differences between the two planetary magnetospheres also exist (see Slavin, 2004 for a recent review). In addition to differences in size in absolute and relative to their respective planetary radii scales, the absence of an atmosphere/ionosphere at Mercury is another important distinction. Despite the lack of an atmosphere, ground based measurements have revealed the presence of clouds of neutral gas (Potter and Morgan, 1985) which are believed to be due to surface sputtering by the impinging solar wind ions. However, it is clear that processes related to magnetosphere-ionosphere coupling are absent at Mercury. Accounting for the differences between the magnetospheres of Earth and Mercury goes beyond the characterization of magnetospheres by the parameter  $D_p$  alone and one must look at the scaling laws governing various magnetospheric processes. In general, these scaling laws may be rooted in plasma physics as well as the system size. For example, the formation of plasmoids (or FTEs) at the magnetopause is tied to the plasma parameters (including interplanetary magnetic field, IMF) determining reconnection rates etc. , while their ultimate size may be tied to the system size and could vary from planet to planet. As another example, we note a recent result by Omidi et al. (2004b) who have demonstrated that formation of the quasi-parallel and quasi-perpendicular portions of the bow shock take place at different values of  $D_p$ . In the case of the quasi-perpendicular shocks, where major portion of the dissipation takes place within the shock layer, they form as early as  $D_p \sim 1$ . On the other hand, the quasi-parallel portion of the shock does not fully develop until  $D_p \sim 30$  because of the important role of wave particle interactions, in the ion foreshock, in the shock dissipation processes.

In this paper, we use the results of global hybrid simulations corresponding to  $D_p = 64$  to discuss the nature of magnetospheric discontinuities at Mercury. While, simulations have been performed for various IMF orientations we will focus on the results corresponding to purely northward or southward IMF due to space limitations. Particular attention is paid to the processes related to magnetopause and its boundary layers and slow shocks in the magnetotail.

## MODEL

The hybrid simulation model utilized in this study is described in detail by Omidi et al. (2004a,b) and a brief overview is given here. In the hybrid model electrons are treated as a massless fluid and ions are treated kinetically through Particle-In-Cell (PIC) methods. The simulations are two-dimensional (X-Y) in space ( $\partial/\partial Z = 0$ ) while all three components of electromagnetic fields and currents are included. The number of cells in X and Y directions are 1200 x 1600 respectively, with uniform cell size of 1 ion skin depth in the solar wind. Total of 32 million particles are present in the simulation domain. A line dipole (see Ogino, 1993) is placed at (X = 500, Y=800) with its axis along the Y direction. A plasma absorbing planet with a radius of 30 ion skin depth is also centered at this point. Initially, the system is immersed in a uniform solar wind type plasma which is continuously replenished from the X = 0 boundary. In this study, we assign values of 0.5 to electron and ion  $\beta$  (ratio of kinetic to magnetic pressure) for the solar wind with Alfvénic Mach number of 5. The ratio of ion plasma to gyrofrequency (the same as the ratio of speed of light to Alfvén velocity) is taken to be 6000. This plasma is allowed to leave the system from the other 3 simulation walls. Similarly, floating boundary conditions for the electromagnetic fields are applied to these boundaries so that waves can leave the system. While various directions of the interplanetary magnetic field (IMF) have been considered, for the sake of brevity the results presented here all correspond to IMF confined in the X-Y plane with northward or southward orientations. The dipole strength corresponds to  $D_p = 64$ . In order to resolve all scales of relevance in the simulations and, at the same time, optimize the computation time the box is divided into two separate zones where both ion motion and electromagnetic fields are solved for using different time steps. Here time step of  $0.0025 \Omega^{-1}$  (inverse ion gyrofrequency) is used in zone-1 and smaller time steps (by varying factors) are used in zone-2 (see Fig.1 in Omidi et al., 2004a). Finally, a uniform resistivity corresponding to resistive length scale of 0.03 ion skin depth is used. Simulations have been run long enough to achieve a semi-steady state solution where the overall structure of magnetospheric regions remain the same. Except for velocity, which is normalized to Alfvén speed in the solar wind, all other plasma and field parameters are normalized to their corresponding solar wind values.

## RESULTS AND DISCUSSION

The two panels in Figure 1 show the plasma density in the entire simulation box for northward (left) and southward (right) IMF orientations. In both cases, the presence of the bow shock, ion foreshock, magnetosheath, magnetopause, cusp, lobe and plasma sheet is evident although the characteristics of these region are quite distinct in the two cases. Starting with the bow shock, the perpendicular orientation of the IMF in both cases leads to a quasi-perpendicular geometry for the dayside and quasi-parallel on the flanks. The presence of density fluctuations in the ion foreshock is evident in both cases although considerable differences between them is also present. In a recent study by Omid *et al.* (2004b) and Blanco-Cano *et al.* (2004) the properties of the bow shock and foreshock ULF waves and ion distribution functions observed in these and simulations with other IMF orientations have been analysed in considerable detail. The results show similarity to the observations at the Earth's bow shock, indicating that Mercury's bow shock operates in a similar fashion. This is understandable in that the shock dissipation processes and properties of the upstream waves are determined by plasma parameters and beyond a point the absolute size of the system does not significantly alter the bow shock related processes. Due to space limitations, we forego a detailed discussion of the bow shock and ion foreshock and refer the reader to the two above mentioned papers. Here we focus on the differences in the bow shocks in Figure 1 and how they relate to bow shock-magnetopause coupling processes.

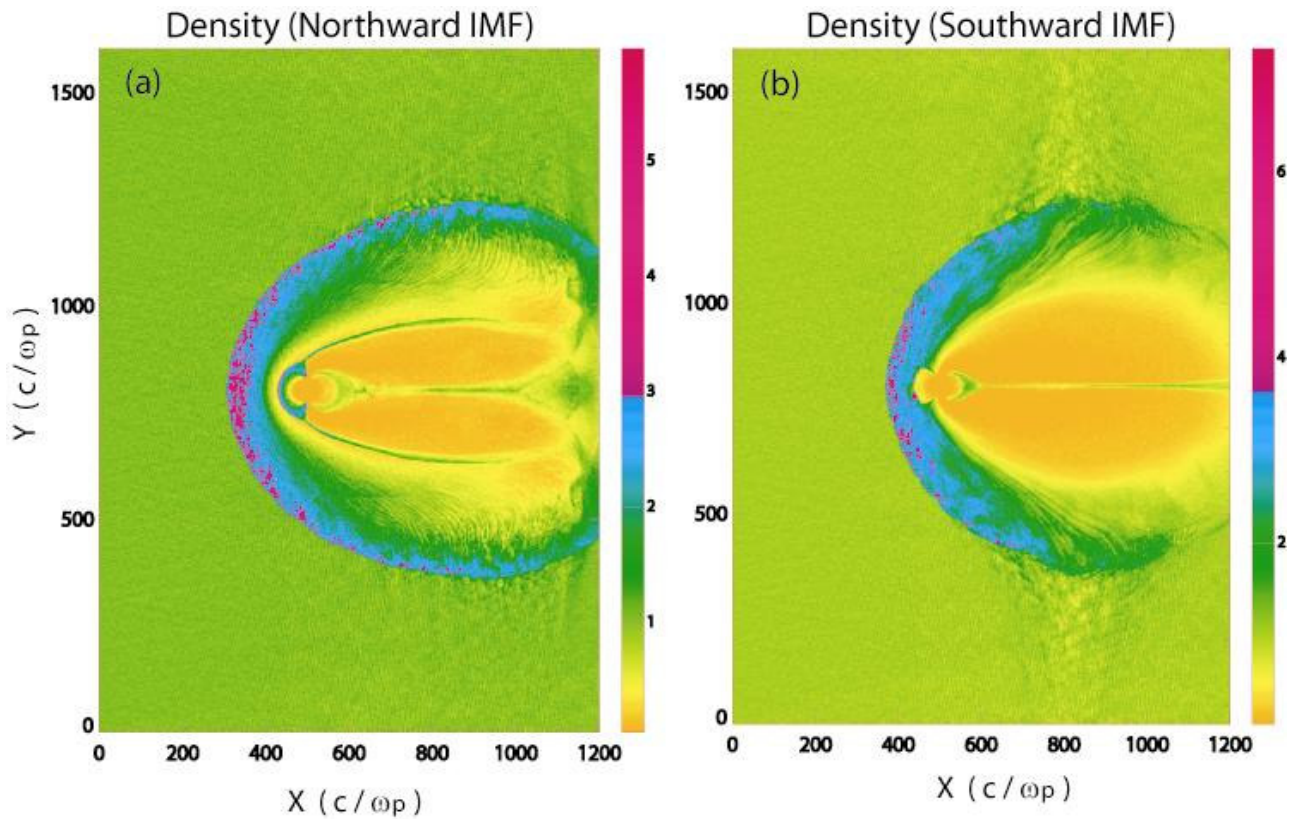


Fig. 1. Density (normalized to solar wind density) as a function of X and Y during (a) northward and (b) southward IMF.

If the magnetopause were to act as a solid obstacle to the solar wind flow, one would expect the bow shocks in Figure 1 to be alike since in both cases the IMF orientation leads to the same bow shock geometry (i.e. quasi-perpendicular at the dayside and quasi-parallel on the flanks). The differences in the two bow shocks, are therefore, tied to the differences in the magnetopause properties during northward and southward IMF. To further illustrate this point we show in Figure 2 time stack plots of density for northward (top panel) and southward IMF cases during the time period  $138 > \Omega T > 125$  in the simulations where  $\Omega$  is the ion gyrofrequency. The time stacks correspond to a cut along the nose bow shock and magnetopause (i.e.  $Y = 800, 480 > X > 250$ ). In these plots, bow shock is identified as “BS”, magnetopause as “MP” and the depletion layer as “DL”. A number of points are evident from Figure 2. One is that the distance between the bow shock and the magnetopause is different in the two cases with the positions of the magnetopauses coinciding and the bow shock in the northward IMF case propagating further upstream. The magnetopause positions correspond to a distance of  $\sim 64$  ion skin depth upstream of the dipole, as one would expect for  $D_p = 64$ . While the bow shock positions have reached a semi-steady state, they are not entirely stationary and propagate upstream. Examination of the flow velocity along the shock normal (i.e. X direction) in the downstream regions shows a stagnant flow ( $V_x \sim 0$ ) when IMF is northward and  $V_x \sim 1 V_A$  (upstream Alfvén speed) when southward. The difference in the downstream speeds can be deduced from the wave phase fronts in the magnetosheath seen in Figure 2 (see Blanco-Cano et al., 2004 for a detailed discussion of these waves) and is directly tied to the fact that in the northward case, the nose magnetopause acts as a solid obstacle and the flow comes to a stop. Whereas, in the southward case magnetic reconnection leads to acceleration away from the nose (to higher latitudes) and the magnetosheath plasma never reaches a stagnant stage (more on this below).

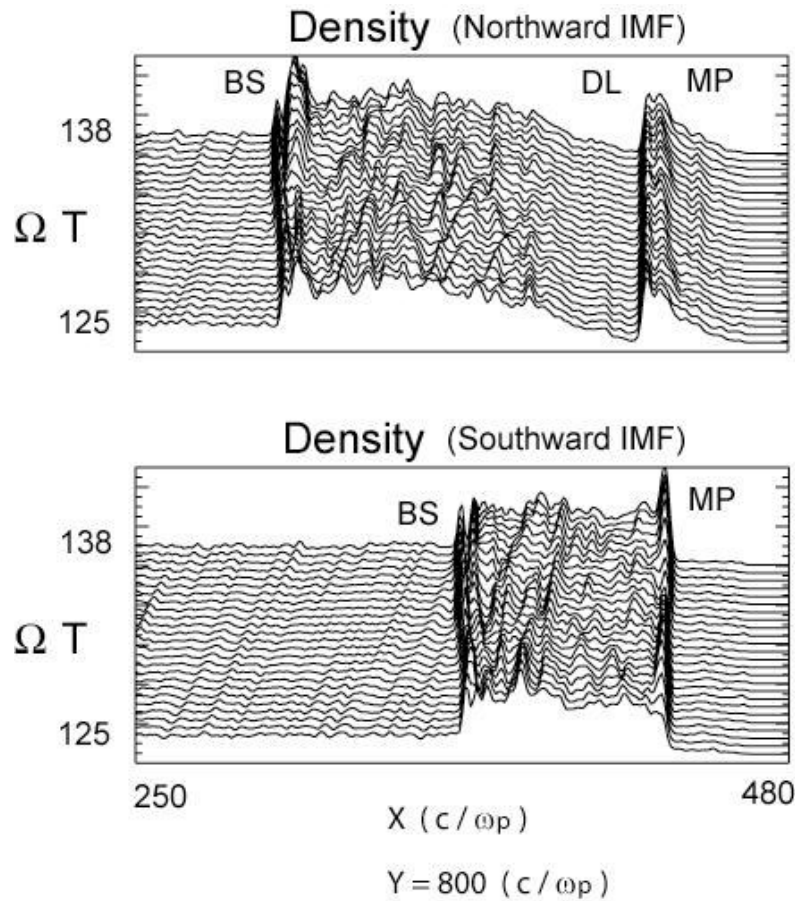


Fig. 2. Time stack of density along the nose bow shock and magnetopause during (top panel) Northward IMF and (bottom panel) southward IMF.

The position of the magnetopause has an implication regarding ion sputtering on Mercury's surface by the solar wind. Based on Mariner 10 observations (Russell, 1977; Ness et al., 1976), the mean distance of Mercury's magnetopause was estimated at  $1.5 R_M$  (Mercury radii), i.e. half the planetary radii above the surface. Using individual magnetopause and bow shock crossings, Slavin and Holtzer (1979) extrapolated subsolar magnetopause distances that varied between  $1.3$  and  $2.1 R_M$  with the lower values occurring during southward IMF and higher values during northward. This variation has been attributed to erosion of magnetic flux on the dayside due to magnetic reconnection during periods of southward IMF. In the case of severe erosion of magnetic flux, the low latitude regions on the surface could be exposed to direct impact of the solar wind leading to ion sputtering. The results shown here do not show any evidence of magnetic erosion occurring during southward IMF despite the presence of magnetic reconnection at low latitude magnetopause (shown below). Using the expected rate of erosion shown in Figure 6 of Slavin (2004) during the current simulation time (1-1.5 min) one would obtain inward motion of the magnetopause by about 3-5 ion skin depth. Future 3-D simulation studies are needed to assess the rate of erosion of magnetic flux and its impact on ion sputtering at Mercury.

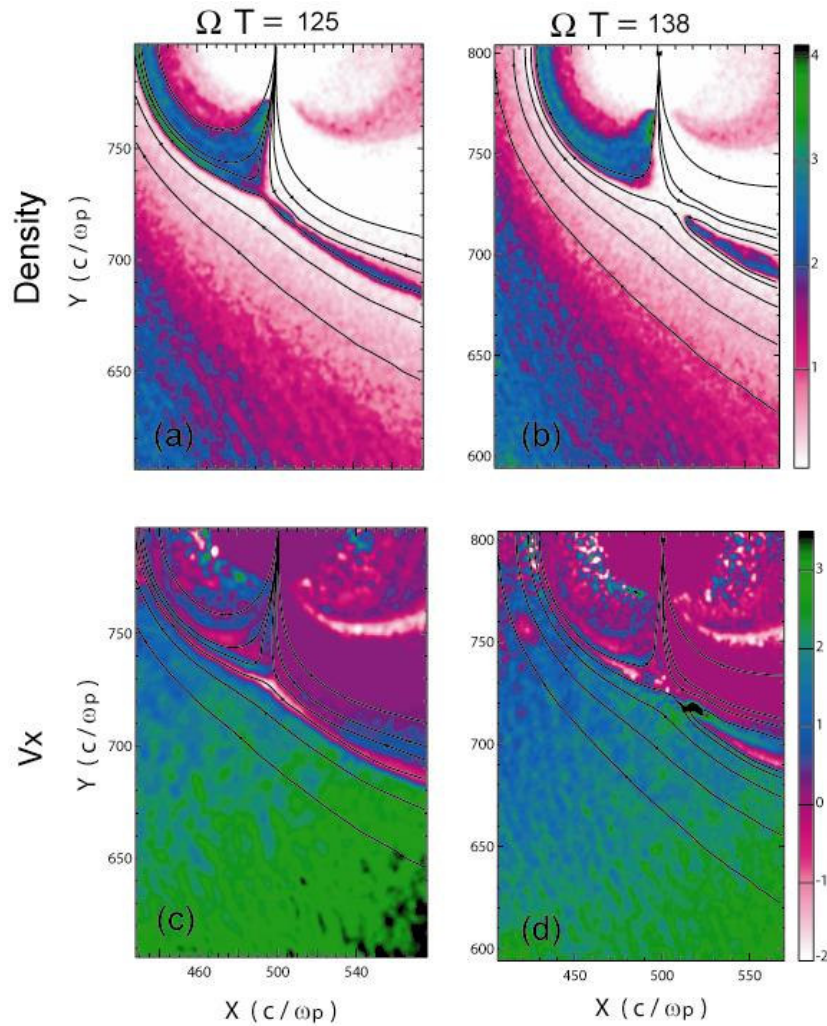


Fig. 3. Density (normalized to solar wind) and flow velocity (normalized to Afven speed in solar wind) at high latitude magnetopause during Northward IMF before and after formation of a new X- line.

It is evident from Figure 2 that while the distance of the subsolar magnetopause is essentially the same during northward and southward IMF, its structure is quite different. The plasma depletion layer is absent during southward IMF and the boundary layer is considerably thinner. In contrast, the boundary layer during northward IMF consists of a peak and a broad shoulder in density. This boundary layer is formed as a result of magnetic reconnection tailward of the cusp region similar to the model proposed by Song and Russell (1992). This is further illustrated in Figure 3 which shows the density, magnetic field lines, and velocity along the X direction zoomed near the southern cusp during northward IMF. The two left panels correspond to time  $\Omega T = 125$  at which an earlier formed X-line has propagated tailwards and out of the zoomed region in the figure. The right hand panels correspond to a later time when a newly formed X-line is present. Examination of panel (c) shows the presence of sunward flowing plasma (pink and white colors) within the high latitude boundary layer (HLBL). This plasma is seen to flow towards low latitudes leading to the formation of a layer within the low latitude boundary layer (LLBL). This layer is adjacent to another with the opposite flow direction originating from the northern HLBL. Particle mirroring and drift results in the formation of multiple layers with opposite flow directions within the boundary layer leading to its broadening. The dynamic nature of the formation and structure of the boundary layer can be seen by comparing the left and the right hand panels in Figure 3. Formation of a newly formed X-line is seen to interrupt or modify the previous flow patterns in the boundary layer as is evident in panels (c) and (d). For example, acceleration of plasma at the reconnection site towards the tail leads to the formation of counterstreaming plasmas in HLBL (panel d) with the sunward component corresponding to the old HLBL plasma seen in panel (c).

The best evidence for the presence of magnetic reconnection at Mercury is the detection of Flux Transfer Events (FTEs) reported by Russell and Walker (1985). Examination of the simulated magnetopause during southward IMF also demonstrates the formation of plasmoids (FTEs). Figure 4 shows the density and flow velocity in the Y direction, zoomed around dayside magnetopause at two different times during the simulation. It can be seen from the field lines in panels (a) and (c) that an X-line is formed at the subsolar magnetopause at  $\Omega T = 125$ . Acceleration of plasma from the X-line towards the higher latitudes (see panel c) leads to the formation of the boundary layer which consists of a large plasmoid in the southern hemisphere and a smaller one at higher latitudes in the northern hemisphere. This boundary layer is on the field lines with one foot on the planet and the other in the solar wind through the quasi-parallel shock. As a result, much of the boundary layer plasma escapes into the ion foreshock enhancing wave-particle interactions in this region. This accounts for the differences (see Figure 1) in the ion foreshock during northward and southward IMF. Thus, we have demonstrated two processes involved in the coupling between the bow shock and the magnetopause. One is the degree of plasma stagnation at low latitude magnetopause which influences the shock strength and its standoff position. The other is the injection of boundary layer plasma into the ion foreshock which ultimately affects the degree of plasma entry into the magnetosphere. Yet another coupling process is through the interaction of shock generated waves and turbulence with the magnetopause possibly influencing the occurrence of reconnection and plasma transport.

Comparison of the left and the right hand panels in Figure 4 reveals information about the formation, as well as, temporal and spatial evolution of plasmoids. Starting with the large plasmoid in the southern hemisphere, a comparison at two different times shows that it has moved along the magnetopause surface to higher latitudes while expanding further in size. The same is also true for the plasmoid in the northern hemisphere. Panels (b) and (d) in Figure 4 also show the generation of a number of new small plasmoids at the magnetopause. This is seen to occur periodically during the run. As they grow in size, further nonlinear evolution of the plasmoids leads to their coalescence and formation of larger plasmoids. The resulting plasmoids can vary in size and account for the differences between the two plasmoids seen in panels (a) and (c) which in turn leads to considerable variation in the thickness of the boundary layer along the surface of the magnetopause. More detailed analysis of the simulation data is needed to ascertain whether the initial formation of a number of small plasmoids is tied to the ion tearing instability or whether the presence of magnetosheath turbulence leads to multiple reconnection sites. The difference in the size of the plasmoids in the northern and southern hemispheres suggests some level of randomness involved in the process which could be attributed to the influences of magnetosheath turbulence on the initial size and further evolution of the plasmoids. However, one cannot rule out the possibility of inherent randomness involved in the nonlinear evolution of plasmoids, by itself accounting for the difference in the size of the plasmoids. In regards to possible differences that may exist between the FTEs observed at Earth and Mercury, it is very likely that the same plasma physical processes are operative at both planets. However, the maximum size of FTEs at Mercury may be smaller than that at Earth by virtue of the fact that the latter provides a larger region for the FTEs to grow.

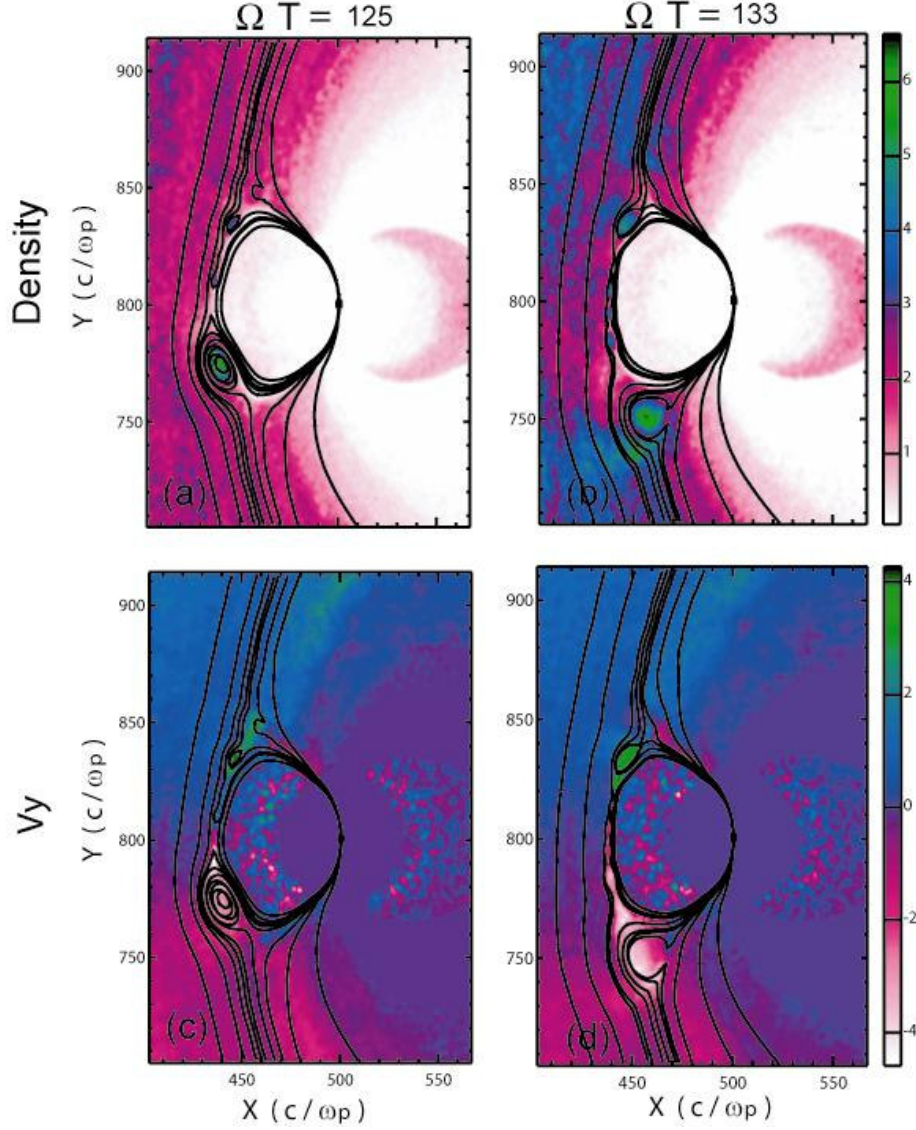


Fig. 4. Density and flow velocity at two different times during Southward IMF showing formation and evolution of plasmoids (FTEs) at the dayside magnetopause.

Comparison between panels (a) and (b) in Figure 1 demonstrate considerable differences in the structure of the magnetotail, among them the presence of two boundaries bifurcating from the end of the plasma sheet during northward IMF. To further investigate the nature of these boundaries, we show in Figure 5 density, total magnetic field strength and field lines, ion temperature and the Y component of velocity along with flow lines. A number of points, in this figure, are evident which all point towards a slow shock interpretation of these boundaries. Namely, the increase in density across the boundaries is associated with a decrease in magnetic field and increase in ion temperature which also leads to the presence of backstreaming ions. These ions follow the lobe field lines towards the planet. The presence of converging plasma (see  $V_y$  and flow lines) upstream of the boundaries and a purely tail ward flow in the downstream is also supportive of a slow shock interpretation. Finally, the bending of the field lines across the boundaries is consistent with slow shock interpretation. These shocks propagate tailward at a speed of  $3 V_A$  and in their trail leave a hot dense plasma in the central part of the tail (i.e. plasma sheet) and a boundary layer plasma, on each side, consisting of the backstreaming ions. The fact that the temperature of the plasma sheet is higher than downstream of the slow shocks suggests the presence of additional compressional heating at the joining point of the two slow shocks.

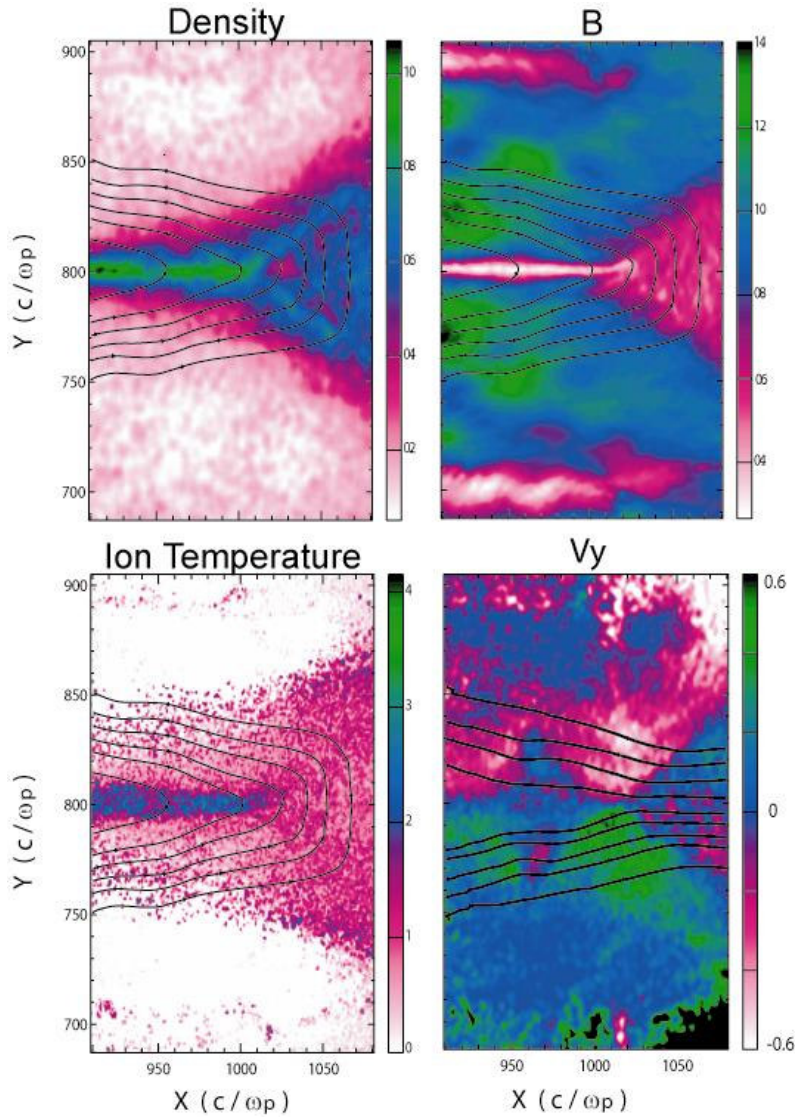


Fig. 5. Plasma and field parameters zoomed near the 2 slow shocks in the magnetotail during northward IMF.

Petscheck's (1964) model of steady state reconnection in the magnetotail, during periods of southward IMF, predicted the existence of pairs of slow shocks emanating from the diffusion region. Observations in the geotail have revealed the presence of slow shocks during both northward and southward IMF (e.g. Feldman et al., 1985). According to Saito et al. (1995), 11% of the plasma sheet/lobe crossings by Geotail spacecraft were associated with slow shocks while Ho et al. (1996) report a 20% value for ISEE-3 crossings. The latter study also found that of the 77 plasmoid events associated with plasma sheet crossings 33 included slow shocks as part of the boundary structure. In short, observations suggest that slow shocks in the tail are generated in more than one way and could be associated with a semi-steady state or a dynamic process. The results shown here, illustrate a way in which a pair of slow shocks can form during northward IMF. These shocks play a critical role in the formation of the plasma sheet and the associated boundary layer. To further illustrate the formation of the slow shocks we show density and  $V_Y$ , at two earlier times during the simulation, in Figure 6. As the solar wind flow begins to pull the dipolar field tailwards a cavity is formed in the tail. The pressure gradient associated with the cavity results in acceleration of plasma towards the central part of the tail. This process is illustrated in the top two panels of the figure. The interaction of these counter streaming plasmas eventually leads to the formation of the slow shocks (bottom panels) which propagate tailward.

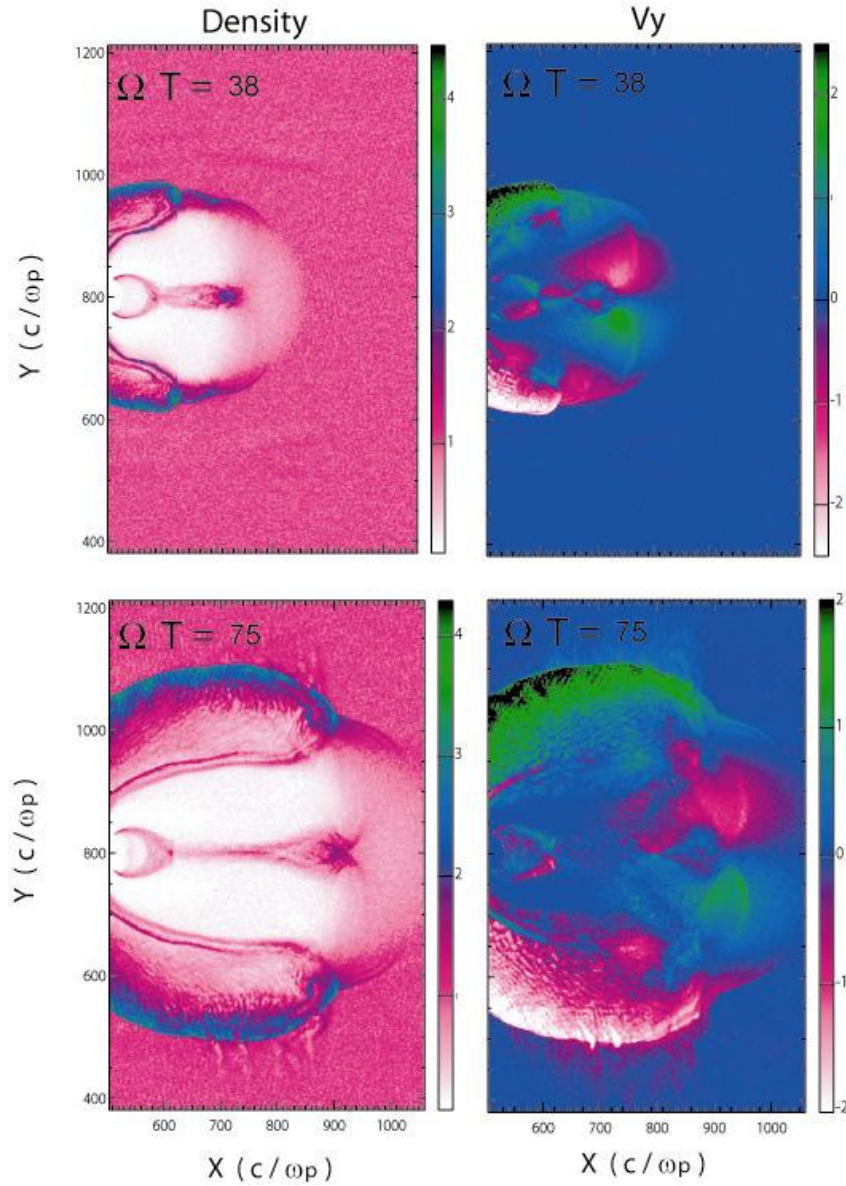


Fig. 6. Density and  $V_Y$  during two early times during the simulation showing the formation of slow shocks in the magnetotail during northward IMF.

The contrast in the tail structures seen in Figure 1, is to a large extent due to the formation of slow shocks during northward IMF. The absence of slow shocks during southward IMF can be explained in a number of ways. One is tied to the size of the simulation box in that the X-line formed in the tail has propagated out of the box and therefore, no slow shocks are emanating from it. Future simulations with larger box size will shed further light on this possibility. It is also possible that the field geometry and plasma conditions are such that slow shocks cannot form. The fact that slow shocks were not present even when the X-line was still in the simulation domain may be consistent with this possibility. Previous, local, 2-D hybrid simulations of slow shocks also support such a possibility (Kauss-Varban and Omidi, 1995; Lin and Swift 1996; Lottermoser et al., 1998; Scholer and Lottermoser, 1998; Cremer and Scholer, 2000). These studies have found a number of different steady-state reconnection solutions for the tail geometry where slow shocks are not part of the solution mostly due to the thinness of the plasma sheet and not enough room for a true downstream to form. Clearly, a lot more remains to be learned about the role of slow shocks in the magnetotail, however, it is evident from the results presented here that slow shocks are expected to be a part of the hermean magnetosphere.

## SUMMARY

We have used the results of 2-D hybrid simulations to characterize the nature of solar wind interaction with Mercury. For the sake of brevity, only the results from cases of purely northward and southward IMF were presented. These simulations illustrate that many of the processes occurring at the Earth's magnetosphere should also be present at the hermean magnetosphere. With regard to the bow shock, foreshock and the magnetosheath a detailed study by Omidi et al. (2004b) and Blanco-Cano et al. (2004) shows that features observed in  $D_p = 64$  simulations resemble those observed at Earth suggesting that Mercury's bow shock should be similar to Earth's. Here we have shown that differences in shock coupling to the magnetopause during northward and southward IMF lead to a thicker magnetosheath during the former case. Specifically, magnetic reconnection during southward IMF diverts the magnetosheath plasma without stagnation at the subsolar magnetopause resulting in a weaker shock. The reconnection accelerated plasma is found to escape into the ion foreshock enhancing the level of ULF waves generated in that region. Formation of multiple plasmoids (FTEs) with varying sizes at the magnetopause during southward IMF was illustrated. The extent to which formation of multiple plasmoids is tied to the ion tearing instability or multiple reconnection sites due to magnetosheath turbulence remains to be further investigated. While FTEs at Mercury and Earth have much in common, their maximum size could be larger at Earth due to availability of more space for FTE's to grow and coalesce. Magnetic reconnection was also shown to be operative tailward of the cusp during northward IMF leading to the formation of low and high latitude boundary layers. Considerable differences in the magnetotail structures during northward and southward IMF were also demonstrated, with a major difference being due to the formation of a pair of slow shocks during northward IMF. These shocks play an important role in the formation of the plasma sheet and the associated boundary layer.

We close by noting that by virtue of being 2-D the results presented here have some limitations that must ultimately be addressed in 3-D simulations. For example, 2-D plasmoids are only an approximation to FTEs which are inherently 3-D in nature. Similarly, with regard to the question of magnetic erosion and the thickness of the magnetosheath 3-D effects need to be accounted for before any firm conclusions can be reached. Despite their limitations, however, 2-D simulations provide much insight and contain many phenomena that exist in 3-D and are easier to first understand from 2-D results. The upcoming missions to Mercury (MESSENGER and BepiColombo) are a great motivation for more detailed 2- and 3-D hybrid simulations in the future and promise to greatly enhance our understanding of the hermean magnetosphere and give us a more comprehensive understanding of its similarities and differences to the terrestrial magnetosphere.

## ACKNOWLEDGMENTS

The work at UCSD was supported by NASA grants NAG5-12946, NAG5-11754 and NSF grant ATM-9901665. The use of multiple-time-grid hybrid code developed by SciberNet Inc. is acknowledged. Computing support by San Diego Supercomputer Center is acknowledged. The work at UCLA was supported by NSF grant ATM01-01145.

## REFERENCES

- Blanco-Cano, X., N. Omidi, C. Russell, H. Karimabadi, "Macrostructure of the bow shock and ion foreshock: Wave properties, *J. Geophys. Res.*, submitted, 2004.
- Cremer and Scholer, *Geophys. Res. Lett.*, 26, 2709, 1999
- Feldman et al., *J. Geophys. Res.*, 90, 233, 1985
- Ho et al., *J. Geophys. Res.*, 101, 15277, 1996

- Krauss-Varban and Omidi, *Geophys. Res. Lett.*, 22, 3271, 1995
- Lin, Y. and D. W. Swift, *J. Geophys. Res.*, 101, 19859, 1996
- Lottermoser et al., *J. Geophys. Res.*, 103, 4547, 1998
- Ness, N.F., Behannon K.W., et al., Magnetic field of Mercury, *J. Geophys. Res.*, 80, 2708-2716, 1975
- Ness, N.F., Behannon K.W., et al., Observations of Mercury's magnetic field, *Icarus*, 28, 479-488, 1976
- Ogilvie, K.W., Scudder, J.D., et al. , Observations at planet Mercury by the electron plasma instrument: Mariner 10, *J. Geophys. Res.*, 82, 1807-1824, 1977
- Ogino, T., Two-dimensional MHD code, in *Computer Space Plasma Physics: Simulations and software*, edited by H. Matsumoto and Y. Omura, pp. 161-191, Terra Scientific Publishing, Tokyo, 1993.
- Omidi, N., X. Blanco-Cano, C. T. Russell, and H. Karimabadi, "Dipolar magnetospheres and their characterization as a function of magnetic moment", *Adv. Space Res.*, 33, Issue 11, 1996, 2004a.
- Omidi, N., X. Blanco-Cano, H. Karimabadi, C. Russell, "Macrostructure of the bow shock and ion foreshock: Scale lengths, *J. Geophys. Res.* , submitted, 2004b.
- Petschek, *NASA Spes. Publ.* , *NASA-sp-50*, 425, 1964.
- Potter, A.E. , Morgan, T.H., Discovery of sodium in the atmosphere of Mercury, *Science*, 229, 651-653, 1985
- Russell, C.T., On the relative locations of the bow shocks of the terrestrial planets, *Geophys. Res. Lett.*, 387-390, 1977
- Russell, C.T., Walker, R.J., Flux transfer events at Mercury, *J. Geophys. Res.*, 90, 11067-11074, 1985
- Russell, C.T., Baker, D.N., Slavin, J.A., The magnetosphere of Mercury, in Chapman, C. (Ed.), *Mercury*, University of Arizona Press, Tucson, pp. 514-561, 1988
- Saito et al., *J. Geophys. Res.*, 100, 23567, 1995
- Slavin, J.A., Holtzer, R.E., The effect of erosion on the solar wind standoff distance at Mercury, *J. Geophys. Res.*, 84, 2076-2082, 1979
- Slavin, J. A., Mercury's Magnetosphere, *Advances in Space Res.*, 33, 1859-1874, 2004
- Scholer, M. , R. F. Lottermoser, *Geophys. Res. Lett.*, 25, 3281, 1998
- Song, P., and C. T. Russell, A model of the formation of the low-latitude boundary layer, *J. Geophys. Res.*, 94, 1411, 1992.

E-mail address of N. Omidi: nomidi@ece.ucsd.edu

Manuscript received X December 200X; accepted X August 200X

